Journal of Magnetic Resonance 203 (2010) 177–184

Contents lists available at ScienceDirect

Journal of Magnetic Resonance

journal homepage: www.elsevier.com/locate/jmr

Interresidue carbonyl–carbonyl polarization transfer experiments in uniformly ^{13}C,^{15}N-labeled peptides and proteins

Rafal Janik [a,b,1], Emily Ritz [a], Andrew Gravelle [a,b], Lichi Shi [a,b], Xiaohu Peng [a,b,2], Vladimir Ladizhansky [a,b,*]

[a] Department of Physics, University of Guelph, 50 Stone Road East, Guelph, Ont., Canada N1G 2W1
[b] Biophysical Interdepartmental Group, University of Guelph, 50 Stone Road East, Guelph, Ont., Canada N1G 2W1

ARTICLE INFO

Article history:
Received 19 November 2009
Available online 24 December 2009

Keywords:
Magic angle spinning
Homonuclear recoupling
Chemical shift anisotropy
Chemical shift correlation spectroscopy

ABSTRACT

In this work, we demonstrate that Homonuclear Rotary Resonance Recoupling (HORROR) can be used to reintroduce carbonyl–carbonyl interresidue dipolar interactions and to achieve efficient polarization transfer between carbonyl atoms in uniformly ^{13}C,^{15}N-labeled peptides and proteins. We show that the HORROR condition is anisotropically broadened and overall shifted to higher radio frequency intensities because of the CSA effects. These effects are analyzed theoretically using Average Hamiltonian Theory. At spinning frequencies used in this study, 22 kHz, this broadening is experimentally found to be on the order of a kilohertz at a proton field of 600 MHz. To match HORROR condition over all powder orientations, variable amplitude radio frequency (RF) fields are required, and efficient direct transfers on the order of 20–30% can be straightforwardly established. Two- and three-dimensional chemical shift correlation experiments establishing long-range interresidue connectivities (e.g., (N[i]–CO[i − 2])) are demonstrated on the model peptide *N*-acetyl-valine-leucine, and on the third immunoglobulin binding domain of protein G. Possible future developments are discussed.

1. Introduction

Solid state NMR (SSNMR) has great potential for studying insoluble biological systems in their native environments. In particular, a few structures of membrane-embedded proteins have been obtained from SSNMR of oriented samples [1–4]. Magic angle spinning (MAS) methods have also been rapidly developing, and a number of very encouraging studies of membrane-associated peptides and proteins have been published in recent years [5–7], including large membrane proteins such as bacterial proton pumps bacteriorhodopsin [8] and proteorhodopsin [9,10], GPCR rhodopsin [11], chimeric potassium channel [12], outer membrane protein G [13,14], disulfide bond forming membrane-associated enzyme DsbB [15], as well as many others.

Many of these studies involve the analysis of multi-dimensional NMR spectra measured in samples with uniform incorporation of ^{13}C and ^{15}N isotopic labels. Obtaining spectroscopic assignments in such samples is the most critical step and the prerequisite for any further site-specific investigation of a macromolecule. In general, the assignment strategies rely on a concerted analysis of intraresidue and interresidue correlation spectra, which yields chemical shifts of individual atoms in all residues. Many techniques for assignments have been proposed in the past decade. They differ, for the most part, in how individual polarization transfer steps are implemented (reviewed in [16]). While for small proteins 2D spectroscopy appear to be sufficient to resolve most sites and establish interresidue connectivities for an uninterrupted backbone walk [17], for larger proteins 3D (and even 4D) chemical shift correlation methods are necessary [9,15,18]. An overwhelming advantage of higher spectral resolution offered by 3D methods is especially critical in large membrane proteins with congested spectra [9,15].

The suite of experiments for spectroscopic assignment is currently limited to those that establish correlations either between atoms located within the same residue (e.g., NCACX experiment), or in the neighboring amino acids (e.g., NCOCX and CONCA experiments). In many cases, these methods need to be assisted by specially designed isotopic labeling techniques, such as reverse labeling [9,19] or alternative labeling [20,21], but in general, it would be beneficial to be able to establish long-range correlations, for example between atoms in residues separated by at least one amino acid. These types of correlations are unlikely to be established through the sequential walk: an obvious drawback of such an approach is its low sensitivity – most of the polarization is lost during the transfers. Assuming that each step is ~50% efficient,

* Corresponding author. Fax: +1 519 836 9967.
E-mail address: vladimir@physics.uoguelph.ca (V. Ladizhansky).
[1] Present address: Imaging Research, Sunnybrook Health Sciences Centre, 2075 Bayview Avenue, Toronto, Ont., Canada M4N 3M5.
[2] Present address: Department of Applied Mathematics, University of Western Ontario, 1151 Richmond St. N., London, Ont., Canada N6A 5B7.

1090-7807/$ - see front matter © 2009 Elsevier Inc. All rights reserved.
doi:10.1016/j.jmr.2009.12.014

about 12–13% polarization transfer efficiency can be achieved in a three-bond transfer experiment. In this publication we propose to use direct carbonyl–carbonyl magnetization transfer steps for establishing long-range interresidue correlations. To the best of our knowledge, N[i]–N[i + 1] is the only type of the direct sequential correlation that has been attempted in the past [22–24]. These experiments require long, on the order of seconds, mixing times. In contrast, efficient inter-carbonyl transfers can be established using short mixing times.

The idea of direct recoupling of $^{13}C'$–$^{13}C'$ dipolar interaction and exploring its dependence on the secondary structure type is, of course, not new and has been used in the past. These measurements are typically performed in samples with selectively introduced carbonyl labels. For instance, Tycko and co-workers [25] have used multiple-quantum non-spinning NMR to detect intermolecular CO–CO interactions to study interstrand arrangement of the full-length $A\beta_{1-40}$ amyloid fibrils. Drobny and co-workers and Mehta et al. have investigated the performance of various recoupling sequences for accurate characterization of peptides' secondary structure [26,27]. More recently, Weliky and co-workers have extended these studies to include fpRFDR [28] (finite pulse radio-frequency driven recoupling) [29].

In our work carbonyl–carbonyl recoupling is used to establish long-range interresidue chemical shift correlations in uniformly ^{13}C,^{15}N-labeled molecules. Carbonyl atoms were chosen because polarization transfer between them can be relatively easily accomplished: (i) CO[i]–CO[i + 1] distances are ~3 Å in a typical α-helix, and a bit longer, ~3.6 Å within β-strands. (ii) Carbonyl resonances are spectroscopically well-separated from the rest of the carbon resonances, in particular from the strongly coupled α-carbons. Band-selective recoupling methods can thus be used to reintroduce CO–CO dipolar couplings without recoupling strong CO–CA interactions and thus avoiding the problem of dipolar truncation. (iii) Carbonyls lack directly bonded protons. This facilitates the use of long recoupling times, even under moderate decoupling conditions. We demonstrate that Homonuclear Rotary Resonance (HORROR) recoupling [30] -based techniques can be used quite effectively for this purpose. We investigate the effect of chemical shift anisotropy on the HORROR recoupling, and show, both theoretically and experimentally, that CSA results in an anisotropic broadening of the HORROR matching condition. This broadening is inversely proportional to the spinning frequency, but remains substantial even at fast MAS rates. Using amplitude-modulated RF fields is required for achieving efficient inter-carbonyl transfers. Finally, we demonstrate that 3D N[i + 1]–CO[i]–CO[i ± 1] correlations can be established in samples of a small microcrystalline protein, the third immunoglobulin binding domain of protein G (GB3).

2. Experimental

2.1. Materials

Two samples were used in this study, *N*-Acetyl-L-Val-L-Leu, and GB3. *N*-Acetyl-[U–^{13}C,^{15}N]-L-Val-L-Leu and natural abundance *N*-acetyl-L-Val-L-Leu were synthesized by American Peptide (Sunnydale, CA). The *N*-Acetyl-[U–^{13}C,^{15}N]-L-Val-L-Leu (NAcVL) sample was diluted to ~8% in the natural abundance NAcVL, and crystallized from aqueous solution by slow evaporation [31]. The crystallized sample was packed into a 3.2 mm diameter rotor for MAS experiments. NAcVL represents the simplest analog of an α-helix with a carbonyl–carbonyl distance of 3.01 Å as determined by X-ray crystallography [31]. This sample was used to test the feasibility of using HORROR for long-range chemical shift correlation experiments, and to investigate the effect of carbonyl CSA on the HORROR spin dynamics.

To further test the feasibility of long-range correlation experiments in proteins a GB3 sample was used. The plasmid encoding GB3 (T1M, T2Q mutant) was kindly provided by Dr. Ad Bax (National Institutes of Health). The expression and purification procedures for GB3 followed those previously published [32–34]. Briefly, GB3 was heterologously expressed in *Escherichia coli* BL21 (DE3) grown in minimal media containing 1 g/L of $^{15}NH_4Cl$ and 2 g/L of ^{13}C-glucose. Expression was induced using 1 mM isopropyl β-D-thiogalactoside (IPTG) and the cells were incubated for 4 h at 37 °C. Disruption of the cell pellet was achieved by two freeze–thaw cycles at −80 °C in phosphate buffered saline (200 mM NaCl, 50 mM Na_2HPO_4, pH 7) and by a subsequent heat treatment at 80 °C for 10 min. The sample was homogenized between freezing cycles using a home-made French press apparatus. The resulting supernatant was concentrated using Amicon Ultra-15 3 kDa MWCO filter (Millipore) and further purified using size exclusion chromatography (Sephadex G-100). Peak fractions were pooled and dialyzed four times against 2 L of distilled water.

The sample was lyophilized and re-dissolved in 50 mM phosphate buffer (pH 6.5) at a concentration of ~40 mg/mL for precipitation. Microcrystals were prepared by dialyzing 330 μL aliquots of the protein solution against a reservoir of 25% isopropanol, 50% 2-methylpentane-2,4-diol at 4 °C for at least 48 h [34]. Approximately 15 mg of precipitated GB3 was packed into a 3.2 mm NMR rotor. Previously published ^{13}C and ^{15}N assignments [34] were confirmed in a series of 2D (^{13}C–^{13}C, NCACX) and 3D NCOCX experiments. Carbonyl shifts are expected to be dependent on the spinning rate [35]. Indeed, at 22 kHz they were found to be slightly different, but generally within 0.4 ppm of the published values.

2.2. NMR spectroscopy

NMR experiments were performed on a narrow bore Bruker Avance III spectrometer operating at 600.013 MHz proton frequency. Experiments on NAcVL were conducted using a 3.2 mm TL2 triple channel $^1H/^{13}C/^{15}N$ MAS probe (Bruker Biospin, MA, USA). A 3.2 mm E-free triple channel $^1H/^{13}C/^{15}N$ MAS probe was used for experiments on GB3. The MAS rate was controlled to within ±2 Hz using a Bruker MAS control unit. The sample temperature was maintained at 271 K in all experiments.

To optimize the transfer efficiency and the decoupling conditions during mixing, a simple one-dimensional spin lock experiment was used. The experiment consisted of an $^1H/^{13}C$ cross-polarization (CP) [36] followed by a spin lock pulse on the ^{13}C channel applied simultaneously with high-power proton decoupling. The performance of continuous wave (CW), two pulse phase modulation decoupling (TPPM) [37], and small phase incremental alteration decoupling (SPINAL-64) [38] were tested during HORROR mixing. CW decoupling showed the best performance, and was thus used in further experiments.

The pulse sequence shown in Fig. 1a was used to investigate the CSA dependence of the HORROR condition, and to determine the effect of the shape of the mixing pulse. In this pulse sequence, the selective Gaussian pulse (90° flip angle, 182 μs duration) following the $^1H/^{13}C$ CP stores carbonyl magnetization along the *z*-axis. Its phase-cycle ensures that carbonyls are the only polarized spins in the beginning of the indirect t_1 evolution. The HORROR polarization transfer is followed by a purge pulse to remove any residual magnetization orthogonal to the HORROR pulse, and to ensure phase sensitive indirect detection. In all experiments, the cross-polarization mixing time was equal to 2.0 ms, with ^{13}C RF field at 50 kHz, and ^1H RF field strength ramped linearly around the $n = 1$ Hartmann–Hahn [39] condition. The ^1H and ^{13}C π/2-pulse lengths were 2.5 μs and 5 μs, respectively. SPINAL-64 decoupling of 78 kHz [38] was used in the indirect and direct dimensions. CW decoupling of 68 kHz was used during HORROR mixing.

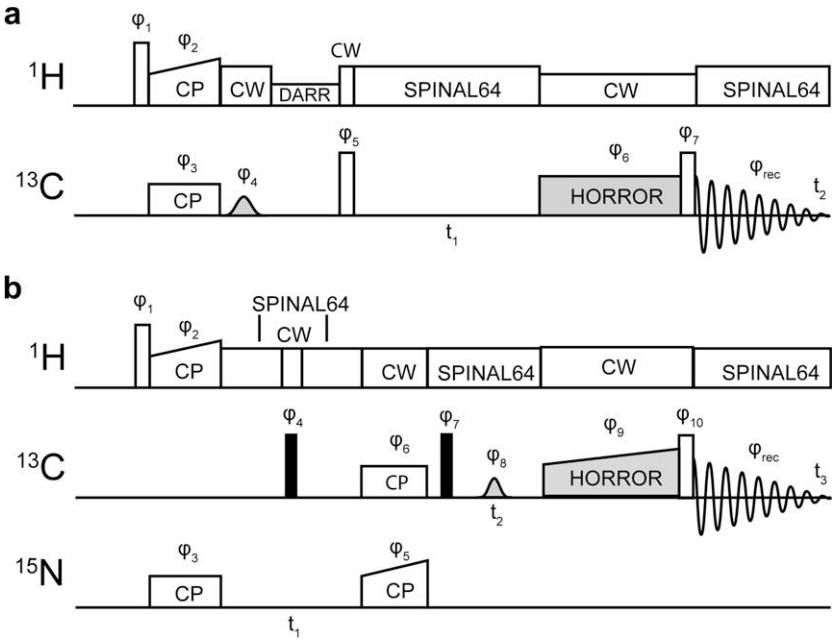

Fig. 1. Experimental pulse sequences. Open and filled rectangles represent 90° and 180° pulses, respectively. (a) 2D CO–CO correlation pulse sequence. Cross-polarization is followed by a pair of 90° selective Gaussian and hard pulses. Both constant power HORROR (as shown in the figure) and amplitude-modulated mixing pulses were used as discussed in the text. The phase-cycle was as follows: $\varphi_1 = 4 \times x, 4 \times (-x)$; $\varphi_2 = y$; $\varphi_3 = x$; $\varphi_4 = y, y, -y, -y$; $\varphi_5 = y$; $\varphi_6 = x, x, -x, -x, -x, -x, x, x$; $\varphi_7 = x, -x$; $\varphi_{rcv} = x, x, -x, -x, -x, -x, x, x$. (b) 3D NCOCO correlation pulse sequence. J_{COCA} homonuclear decoupling is implemented using off-resonance 180° selective Gaussian pulse centered at 50 ppm. The phase cycle was as follows: $\varphi_1 = x$; $\varphi_2 = -y$; $\varphi_3 = x, -x$; $\varphi_4 = y$; $\varphi_5 = x$; $\varphi_6 = \varphi_7 = \varphi_9 = x, x, x, x, y, y, y, y$; $\varphi_8 = x, -x, -x, x, y, -y, -y, y, -x, x, x, -x, -y, y, y, -y$; $\varphi_{10} = x, x, -x, -x, y, y, -y, -y$; $\varphi_{rcv} = x, -x, x, -x, y, -y, y, -y$.

The 3D pulse sequence in Fig. 1b establishes long-range N[i]–CO[i − 1]–CO[i − 2] correlation in addition to the short-range N[i]–CO[i − 1]–CO[i] and N[i]–CO[i − 1]–CO[i − 1] correlations. Briefly, band-selective ^{15}N[i]/^{13}C′[i − 1] cross-polarization [40] is followed by CO[i − 1] chemical shift evolution, which is implemented with off-resonance *J*-decoupling [41]. The following ramped HORROR transfer results in the formation of two cross-peaks of negative intensity, N[i]–CO[i − 1]–CO[i − 2] and N[i]–CO[i − 1]–CO[i], in addition to the pseudo-diagonal N[i]–CO[i − 1]–CO[i − 1] positive peak. HORROR mixing time was of 30 ms duration, with ramp width of ∼1.1 kHz as required to cover anisotropically broadened matching profile (discussed in the following). Other experimental parameters were as follows. The cross-polarization ^{1}H/^{15}N mixing time was set to 2.0 ms, with ^{15}N RF field of 40 kHz, and with ^{1}H RF field strength ramped linearly around the $n = 1$ Hartmann–Hahn condition. ^{15}N/^{13}C′ band-selective cross-polarization was accomplished with ^{15}N RF field of 32 kHz, and with ^{13}C RF filed ramped linearly around the $n = 1$ Hartmann–Hahn condition. CW ^{1}H proton decoupling field of ∼62 kHz was used during ^{15}N/^{13}C′ CP (optimized experimentally). Other acquisition parameters were as follows. For a 2D CO–CO correlation in GB3 (Fig. 1a), 96 points were collected in the indirect t_1 dimension (total acquisition length of 7.95 ms). Each point was averaged over 16 scans with a recycle delay of 2.2 s. For the 3D NCOCO experiment (Fig. 1b) 72 and 136 points were collected in the indirect t_1 and t_2 dimensions, with total acquisition lengths of 11.84 ms and 7.56 ms, respectively. Each FID was averaged over 16 scans, collected with 1.7 s recycle delay.

Pulse sequences shown in Fig. 1 produce both positive and negative peaks. Overlap between them often causes problems with phasing the spectra. To find the correct phasing parameters, we collected additional 2D spectra with HORROR power level sufficiently mismatched to avoid any CO–CO transfer. Specifically, we have used the pulse sequence of Fig. 1a to record an additional 2D ^{13}C′–^{13}C′ spectrum with HORROR power level set to avoid CO–CO recoupling. Such experiment produces a spectrum with diagonal peaks of positive intensity and can be easily phased. Similarly, to determine correct phasing parameters for the 3D NCOCO experiment of Fig. 1b, we have recorded two 2D ^{15}N(t_1)–^{13}C(t_3) and ^{13}C(t_2)–^{13}C(t_3) correlation planes using the same pulse sequence but with mismatched HORROR condition. These experiments do not produce negative peaks, but otherwise have identical phasing properties to those of the full 3D NCOCO.

The 2D and 3D spectra were processed using NMRpipe [42], and analyzed using CARA software [43]. All chemical shifts were indirectly referenced to 2,2-dimethyl-2-silapentane-5-sulfonic acid (DSS) by setting the downfield ^{13}C resonance peak shift of adamantane to 40.48 ppm [44].

3. Theory

Our approach to accomplish the direct carbonyl–carbonyl transfer and to establish long-range correlations is based on the HORROR effect [30]. This method was chosen for its chemical shift selectivity, which ensures that the carbonyls would not recouple to the directly bonded alpha-carbons, and on its relatively low power requirements, which allow high MAS rates without greatly stressing the NMR hardware. The HORROR [30] and related DREAM (dipolar recoupling enhanced by amplitude modulation) [45,46] experiments have been successfully demonstrated on strongly coupled systems of directly bonded carbon atoms. In comparison, the dipolar coupling between adjacent carbonyls is approximately an order of magnitude weaker, and large chemical shift anisotropies of these atoms have a profound effect on the spin dynamics. We therefore begin with the derivation of the effective Hamiltonian using second-order Average Hamiltonian Theory [47], which directly accounts for the CSA effects.

3.1. The effective average Hamiltonian

We first begin by formulating a Hamiltonian for a two-spin system subjected to a through-space dipolar interaction, chemical shift anisotropies (CSA), and under constant RF irradiation:

$$H(t) = \omega_{\mathrm{rf}}(S_x + I_x) + \omega_S(t)S_z + \omega_I(t)I_z + \omega_d(t)\left(3I_zS_z - \vec{I}\cdot\vec{S}\right). \quad (1)$$

The first term in this expression describes the RF field, the second and the third terms are the chemical shift anisotropies of spins with time-dependent CSA coefficients $\omega_S(t)$ and $\omega_I(t)$. The last term is the dipolar interaction characterized by its time-dependent interaction strength, $\omega_d(t)$. The chemical shifts and dipolar interactions can be conventionally represented as Fourier series

$$\omega_A(t) = \sum_{m=-2}^{m=2} \omega_A^{(m)} e^{im\omega_r t} \quad (2a)$$

$$\omega_d(t) = \sum_{m=-2}^{m=2} \omega_d^{(m)} e^{im\omega_r t}, \quad (2b)$$

where $\omega_A^{(m)}$ and $\omega_d^{(m)}$ are orientation-dependent chemical shift ($A = I, S$) and dipolar Fourier coefficients, respectively. Their dependence on the crystallite orientation can be found elsewhere [48]. To simplify the discussion, we neglect the isotropic chemical shifts, i.e., $\omega_A^{(0)} = 0$ in Eq. (2a). We rewrite the Hamiltonian in a tilted coordinate system where the z-axis is aligned with the direction of the RF field. The tilted frame Hamiltonian can be written as

$$H_T(t) = \omega_{\mathrm{rf}}(S_z + I_z) - \omega_S(t)S_x - \omega_I(t)I_x + \omega_d(t)\left(3I_xS_x - \vec{I}\cdot\vec{S}\right), \quad (3)$$

or, using fictitious spin $-1/2$ operators [49,50], can be expressed as

$$H_T(t) = 2\omega_{\mathrm{rf}}I_z^{14} - \omega_S(t)(I_x^{13} + I_x^{24}) - \omega_I(t)(I_x^{12} + I_x^{34}) + \omega_d(t)\left(\frac{3}{2}I_x^{14} + \frac{1}{2}I_x^{23} - \frac{1}{4}(N^{14} - N^{23})\right). \quad (4)$$

Here, N^{14} and N^{23} are the identity matrices in the (1–4) and (2–3) subspaces. The Hamiltonian of Eq. (4) is schematically represented in Fig. 2, using the usual basis set of the product eigenstates of the S_z, I_z operators. The energies of these states are given by the time-independent RF part of the Hamiltonian: $E_{\alpha\alpha} = \omega_{\mathrm{rf}}$, $E_{\alpha\beta} = E_{\beta\alpha} = 0$, $E_{\beta\alpha} = -\omega_{\mathrm{rf}}$. Periodically time-dependent CSA and dipolar Hamiltonians couple the states, and can generate transitions between them if the energy differences between the pairs of coupled states approximately match the modulation frequencies, ω_r or $2\omega_r$, in the CSA and dipolar Hamiltonians. In particular, single-quantum recoupling of the CSA occurs when the frequencies of the single-quantum transitions between the pairs of states $|\alpha\alpha\rangle$ and $|\alpha\beta\rangle$, $|\alpha\beta\rangle$ and $|\beta\beta\rangle$, $|\beta\alpha\rangle$ and $|\alpha\alpha\rangle$, and $|\beta\alpha\rangle$ and $|\beta\beta\rangle$ match ω_r, or $2\omega_r$: $\omega_{\mathrm{rf}} \sim n\omega_r$, $n = 1, 2$ [51].Similarly, double-quantum (DQ) recoupling occurs when the DQ transition frequency matches modulation frequency in the dipolar Hamiltonian: $E_{\alpha\alpha} - E_{\beta\beta} = 2\omega_{\mathrm{rf}} \sim n\omega_r$, $n = 1, 2$. Matching the $n = 1$ condition constitutes the HORROR effect. To derive an effective Hamiltonian for this case, we are going to assume that the RF strength approximately satisfies the HORROR condition, i.e., $\delta = 2\omega_{\mathrm{rf}} - \omega_r$ is small. We first transform the Hamiltonian of Eq. (4) to the interaction frame defined by the transformation operator $U = e^{-i\omega_r I_z^{14} t}$, so that the interaction frame Hamiltonian is represented as:

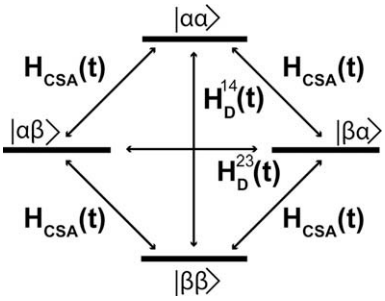

Fig. 2. Schematic representation of the Hamiltonian of Eq. (4). Four energy levels result from the time-independent diagonal part of the Hamiltonian. The states are coupled by the time-dependent dipolar and CSA Hamiltonians as indicated by arrows. In the absence of CSA, the HORROR effect occurs when the energy difference between the $|\alpha\alpha\rangle$ and $|\beta\beta\rangle$ states $E_{\alpha\alpha} - E_{\beta\beta} = 2\omega_{\mathrm{rf}}$ matches the frequency of the first Fourier component of the dipolar interaction, $2\omega_{\mathrm{rf}} = \omega_r$. CSA Hamiltonian can induce single-quantum transitions. As shown in the text, this effect is equivalent to the shift and anisotropic broadening of the HORROR matching condition.

$$\widetilde{H}(t) = \widetilde{H}_0 + \widetilde{H}_D(t) + \widetilde{H}_{\mathrm{CSA}}(t), \quad (5a)$$

where

$$\widetilde{H}_0 = \frac{3}{4}\omega_d^{(-1)}I_+^{14} + \frac{3}{4}\omega_d^{(1)}I_-^{14} + \delta I_z^{14}, \quad (5b)$$

$$\widetilde{H}_{\mathrm{CSA}}(t) = -\sum_{m=-2}^{2} \omega_S^{(m)} e^{im\omega_r t}\left(\left(I_x^{13} + I_x^{24}\right)\cos\left(\frac{\omega_r t}{2}\right) - \left(I_y^{13} + I_y^{24}\right)\sin\left(\frac{\omega_r t}{2}\right)\right) - \sum_{m=-2}^{2} \omega_I^{(m)} e^{im\omega_r t}\left(\left(I_x^{12} + I_x^{34}\right)\cos\left(\frac{\omega_r t}{2}\right) - \left(I_y^{12} + I_y^{34}\right)\sin\left(\frac{\omega_r t}{2}\right)\right), \quad (5c)$$

$$\widetilde{H}_D(t) = \sum_{m=-2}^{2} \omega_d^{(m)} e^{im\omega_r t}\left(\frac{1}{2}I_x^{23} - \frac{1}{4}\left(N^{14} - N^{23}\right)\right) + \frac{3}{4} \times \sum_{\substack{m=-2 \\ m\neq -1}}^{2} \omega_d^{(m)} e^{i(m+1)\omega_r t} I_+^{14} + \frac{3}{4}\sum_{\substack{m=-2 \\ m\neq 1}}^{2} \omega_d^{(m)} e^{i(m-1)\omega_r t} I_-^{14}. \quad (5d)$$

When the CSA is neglected, the zeroth-order Hamiltonian dominates the spin dynamics:

$$\overline{H}^{(0)} = \frac{3}{4}\omega_d^{(-1)}I_+^{14} + \frac{3}{4}\omega_d^{(1)}I_-^{14} + \delta I_z^{14}. \quad (6)$$

It operates in the (1–4) DQ subspace, and couples states $|\alpha\alpha\rangle$ and $|\beta\beta\rangle$, causing double-quantum transition so long as the energy separation between these states, δ, does not greatly exceed the effective coupling strength, $|\frac{3}{2}\omega_d^{(1)}|$. The greatest transfer efficiency occurs when the two levels become degenerate, i.e., when the HORROR condition is exactly satisfied, $\omega_{\mathrm{rf}} = \frac{1}{2}\omega_r$. Eq. (6) then simplifies to the effective Hamiltonian presented in the original study of the HORROR effect [30].

To account for the effect of CSA, we will need to consider the next term in the average Hamiltonian. For small dipolar interactions (two carbonyls separated by ~3 Å), the main contribution will be from the CSA autocorrelation, which results in the additional offset term:

$$\overline{H} = \overline{H}^{(0)} + \overline{H}^{(1)} = \frac{3}{4}\omega_d^{(-1)}I_+^{14} + \frac{3}{4}\omega_d^{(1)}I_-^{14} + \left(\delta - \Delta_{\mathrm{CSA}}^{(14)}\right)I_z^{14} - \Delta_{\mathrm{CSA}}^{(23)}I_z^{23}, \quad (7)$$

where the corrections resulting from the CSA autocorrelation are:

$$\Delta_{\mathrm{CSA}}^{(14)} = \frac{1}{\omega_r}\left(\frac{2}{3}\left(\left|\omega_S^{(1)}\right|^2 + \left|\omega_I^{(1)}\right|^2\right) + \frac{2}{15}\left(\left|\omega_S^{(2)}\right|^2 + \left|\omega_I^{(2)}\right|^2\right)\right)$$
$$\Delta_{\mathrm{CSA}}^{(23)} = \frac{1}{\omega_r}\left(\frac{2}{3}\left(\left|\omega_S^{(1)}\right|^2 - \left|\omega_I^{(1)}\right|^2\right) + \frac{2}{15}\left(\left|\omega_S^{(2)}\right|^2 - \left|\omega_I^{(2)}\right|^2\right)\right). \quad (8)$$

The diagonal part of the Hamiltonian operating in the zero-quantum (2–3) subspace does not cause any time evolution, and the spin dynamics are still controlled by the double-quantum part of the average Hamiltonian, albeit the degeneracy between $|\alpha\alpha\rangle$ and $|\beta\beta\rangle$ states occurs when

$$\omega_{\mathrm{rf}} = \frac{1}{2}\left(\omega_r + \Delta_{\mathrm{CSA}}^{(14)}\right). \quad (9)$$

Eq. (9) establishes the modified HORROR matching condition in the presence of CSA. It occurs at higher RF powers because the CSA correction, $\Delta_{\mathrm{CSA}}^{(14)}$, is always positive. The shift is

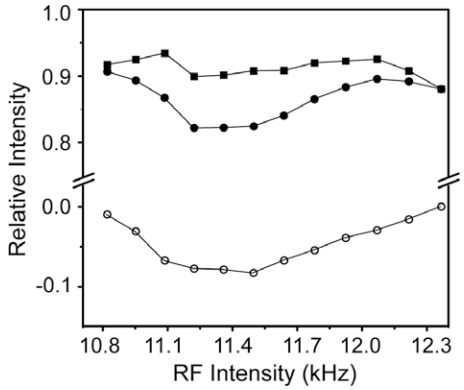

Fig. 3. Experimental HORROR transfer efficiency as a function of RF intensity. Twelve two-dimensional CO–CO correlation experiments were conducted at varying spinning rates to screen the HORROR condition. The HORROR mixing time was set to 20 ms and the experiments were acquired with 52 increments in the t_1 dimension in 16 scans. All intensities are normalized per the intensity of the diagonal peak without mixing. Open circles represent the intensities of the L′–V′ cross-peak, solid circles are the intensities of the L′–L′ diagonal peak, and squares represent the difference. Solid lines are guides to the eye.

orientation-dependent, and is thus anisotropically broadened in a powder sample. This broadening is inversely proportional to the spinning frequency, but remains non-negligible even at fast spinning frequencies.

4. Experimental results and discussion

4.1. Investigation of CSA effects on HORROR transfer

To experimentally investigate the effect of CSA on the width of the HORROR condition in the inter-carbonyl recoupling, a series of two-dimensional CO–CO correlation experiments were conducted on NAcVL using the pulse sequence of Fig. 1a. In these experiments, the constant amplitude RF field was applied to carbons during mixing, and the recoupling efficiency was measured as a function of the RF field strength. The spinning frequency was 22 kHz in all experiments. For HORROR recoupling between spins without CSA, one expects maximum efficiency exactly at $\omega_{rf} = 1/2\omega_r$ with the width of the matching condition on the order of the effective coupling strength, roughly 100 Hz. Fig. 3 shows the normalized integrated intensities of the L′–V′ cross-peaks (open circles) and the L′–L′ diagonal peaks (filled circles). A typical 2D CO–CO correlation spectrum of NAcVL is shown in Fig. 4a. In a qualitative agreement with predictions of Eq. (9), the matching condition is significantly broadened because of the CSA effects: non-negligible polarization transfers could be observed over a range of RF intensities, overall shifted to higher RF fields and almost a kilohertz wide. The maximum achieved intensities were on the order of 7%, much lower than anticipated without CSA.

4.2. Optimization of HORROR transfer efficiency

Because of the CSA-induced broadening, generating efficient transfer between two carbonyls requires matching HORROR conditions for all crystallite orientations in a powder, which can be accomplished through the application of amplitude-modulated RF field. We have investigated the effect of the amplitude modulation on the efficiency of the HORROR mixing for both linearly ramped shapes of 0.22, 0.55, and 1.1 kHz width, centered around 11.5 kHz, as well as for a series of tangential shapes of 0.55, 1.1, and 1.65 kHz width.

The shaped pulse transfer efficiencies were again examined using the pulse sequence of Fig. 1a. A representative 2D carbonyl–carbonyl correlation spectrum collected with a 1.1 kHz wide mixing pulse of 30 ms is shown in Fig. 4a. Overall, the highest transfer efficiencies were measured for the 1.1 kHz linear ramp and for the 1.65 kHz tangentially shaped mixing pulses and were 0.33 and 0.31, respectively. A comparison of different 1D traces for ramped pulses of different widths are shown in Fig. 4b.

In its factual implementation, the ramped HORROR experiments are identical to the DREAM experiment. The latter, however usually refers to experiments with (nearly) adiabatic transfer. We would like to point out that achieving adiabatic transfer over the entire powder distribution in a CO–CO spin pair is hardly possible under our experimental conditions (600 MHz magnetic field, 22 kHz spinning rate). Indeed, the requirement for achieving adiabatic polarization transfer is that the passage through the matching condition is slow enough, so the adiabaticity parameter a_{IS} is much larger than 1 [45]:

$$a_{IS}(T) = \frac{\sqrt{(\Delta_I(T) + \Delta_S(T))^2 + (d'_{IS}(T))^2}}{|d\Theta_{IS}(T)/dT|} \gg 1. \quad (10)$$

In Eq. (10) we used notations introduced in Ref. [45]. T describes time course of the RF modulation during mixing, $\Delta_I(T)$ and $\Delta_S(T)$

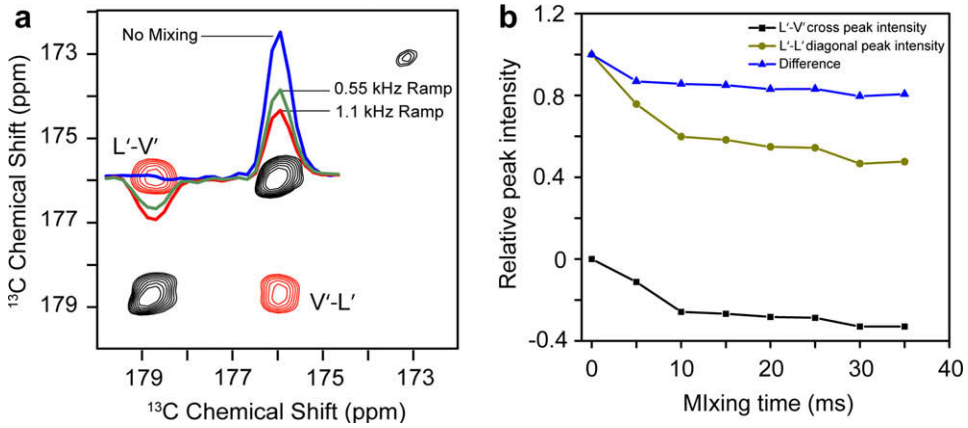

Fig. 4. (a) Two-dimensional CO–CO correlation experiment with 1.1 kHz ramped HORROR pulse of 30 ms. The positive, diagonal (black) peaks represent the remaining polarization, while the negative, cross-peaks (red) represent the transferred signal. One-dimensional traces represent effects of the width of ramp of the mixing pulses on the transfer efficiency. The blue trace corresponds to the experiment without mixing, and is used to normalize the intensities of all other experiments. In green is a result of 0.55 kHz ramp pulse with a maximum transfer efficiency of 19%. In red is the result of 1.1 kHz ramp with an optimal mixing time of 30 ms and a maximum transfer efficiency of 33%. (b) Transfer efficiency as a function of mixing time for 1.1 kHz linear ramp mixing pulse. (For interpretation of the references to color in this figure legend, the reader is referred to the web version of this paper.)

are time-dependent deviations from the HORROR condition for spins I and S, $d'_{IS}(T)$ is the effective dipolar interaction strength, and $\Theta_{IS}(T) = \tan^{-1}(d'_{IS}/2\Delta(T))$ is the angle between the effective Hamiltonian and the z-axis of the DQ subspace. We can neglect any offsets, so the deviations $\Delta_I(T) = \Delta_S(T) = \Delta(T)$, and $d'_{IS}(T) = -\frac{3}{2}\left|\omega_d^{(1)}\right|$.

To achieve adiabatic population exchange, the passage should be slow enough across the entire CSA-broadened HORROR condition. This requires that the rate of passage be at least $d\Delta/dT \ll d'^2_{IS}/2$. For two carbonyl atoms 3 Å apart, $d'_{IS} < 150$ Hz, so the rate of passage should be $d\Delta/dT \ll 11,250\ \mathrm{s}^{-2}$. At 600 MHz proton field and 22 kHz MAS rate the CSA-induced anisotropic broadening is on the order of 1 kHz (Fig. 3), which defines the minimal width of the passage. Assuming a linearly changing RF field, $\Delta(T) = \alpha T$, the minimal time required to establish adiabatic transition across the entire powder needs to be longer than ~100 ms. Due to hardware limitations these mixing times could not be safely achieved. Further prospects for establishing adiabatic transfer will be discussed in the following sections.

4.3. Long-range correlation experiments in GB3

To further investigate the possibility of the interresidue carbonyl–carbonyl transfer, we repeated the experiment of Fig. 1a in the U–^{13}C,^{15}N sample of GB3. The optimal HORROR sweep, duration, and CW decoupling values were the same as those calibrated using the NAcVL sample. A 2D CO–CO correlation spectrum is shown in Fig. 5. We expect to see 55 backbone correlations corresponding to internuclear carbonyl–carbonyl distances in the range of 2.97–3.64 Å for α-helical and β-sheet structures, respectively. In addition, some intraresidue backbone-side chain correlations in Asp, Asn, Gln, and Glt may also show up in the spectra. Although it is quite evident from the figure that inter-carbonyl polarization transfers can be easily established, any quantitative analysis is precluded by the significant spectral overlap. Because the experiment correlates atoms of the same type, most of the cross-peaks occur

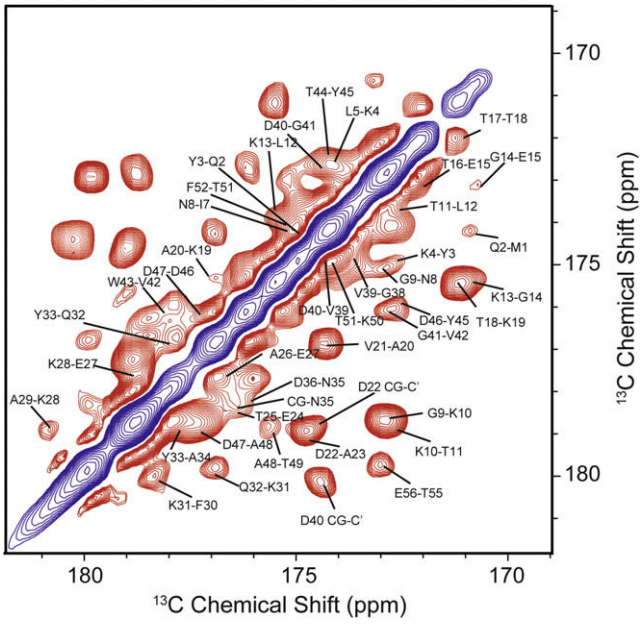

Fig. 5. Two-dimensional CO–CO correlation spectrum collected using pulse sequence in Fig. 1a with 1.1 kHz wide ramped HORROR pulse of 30 ms to 2048(t_1), and 4096(t_2) prior to Fourier transform, and processed with Lorentzian-to-Gaussian apodization function (30 Hz of Lorentzian line narrowing and 60 Hz of Gaussian line broadening) in both dimensions. First contour level was cut at 4.5 times the noise rms, and each next level was multiplied by 1.2.

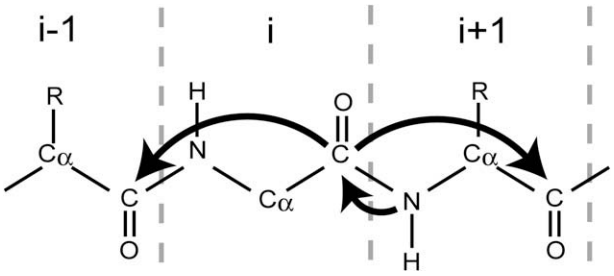

Fig. 6. Schematic representation of the polarization transfer pathways of the NCOCO experiment. This experiment results in three types of cross-peaks. The pseudo-diagonal N[i + 1]–CO[i]–CO[i] cross-peak involves a single polarization transfer and is positive. The N[i + 1]–CO[i]–CO[i + 1] and N[i + 1]–CO[i]–CO[i − 1] cross-peaks result from the long-range CO–CO mixing step and have negative intensities. The latter correlates atoms located in residues separated by two amino acids.

on or close to the diagonal, and result in partial cancelation of the diagonal intensity, with only about 16 cross-peaks sufficiently resolved. By examining the few well separated peaks, a lower bound of 20% was found for the maximum transfer efficiency, but because of the overlap, the maximum transfer efficiency could not be measured more accurately. Nor could we compare the transfer efficiency for residues found in α-helices and β-sheets.

Further attempts to improve the spectral resolution and quantitatively assess the HORROR transfer efficiency in GB3 must rely on the 3D spectroscopy. For example, by dispersing the 2D CO–CO plane according to the ^{15}N chemical shifts of directly bonded nitrogen atoms, most off-diagonal or near-diagonal overlaps are eliminated. Such an NCOCO experiment employs the pulse sequence of Fig. 1b, and results in three types of cross-peaks: a positive "pseudo"-diagonal N[i + 1]–CO[i]–CO[i] correlation, and two negative N[i + 1]–CO[i]–CO[i + 1] and N[i + 1]–CO[i]–CO[i − 1] correlations (Fig. 6).

From the three the latter is a long-range cross-peak that correlates the chemical shifts of atoms that are separated by two residues.

From the expected 109 backbone correlations in GB3 around 80 peaks are expected to be sufficiently resolved in the 3D NCOCO spectrum, and 66 of them can indeed be reliably detected. A representative two-dimensional plane of the NCOCO experiment is shown in Fig. 7.

A number of well-resolved long-range correlations can be seen in this plane, in particular K31N-F30C′-A29C′, E32N-K31C′-F30C′, Y33N-E32C′-K31C′ correlations, belonging to a contiguous stretch A29-F30-K31-E32-Y33. All these residues are located within an α-helical structure with short inter-carbonyl distances on the order of 3 Å. On the other hand, the appearance of two cross-peaks E15N-G14C′-K13C′ and E15N-G14C′-E15C′ is more surprising as these peaks correspond to residues within β-strand with longer inter-carbonyl distances of ~3.65 Å according to the crystal structure [52].

In general, based on the analysis of well-resolved peaks (Table 1) we have not found any significant correlation between the type of secondary structure and cross-peak intensities. We thus conclude that the direct inter-carbonyl connectivities can be established in both α-helices and β-sheets.

Some expected cross-peaks could not be detected in the spectra. In particular, we have not detected any interresidue cross-peaks from the four-residue stretch Y45-D46-D47-A48 located at the end of the β3 strand, and in the following β-turn. In addition, inter-carbonyl cross-peaks from the preceding residues V42, W43 and T44 (e.g., W43N-V42C′-W43C′, T44N-W43C′-T44C′, etc.) were the weakest among all with typical signal-to-noise of ~−7 (Table 1). One possible explanation is that this part of the protein is affected by local motions, which result in averaging of dipolar

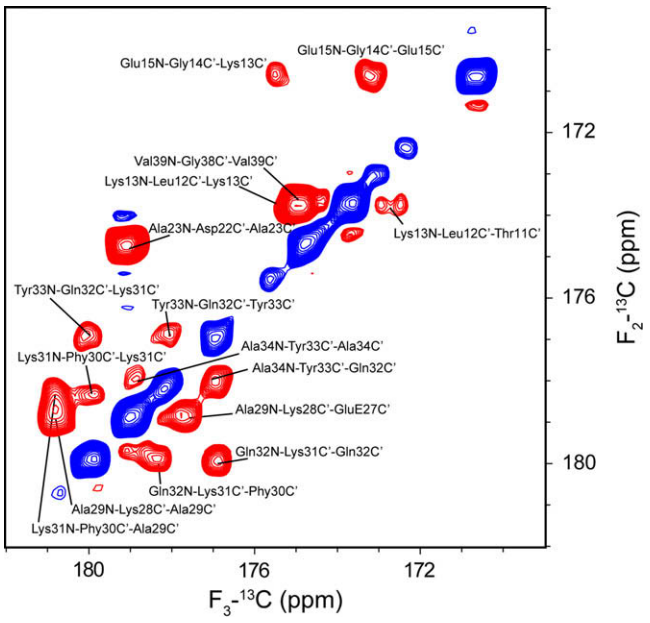

Fig. 7. 2D CO–CO chemical shift correlation plane from a 3D NCOCO correlation experiment extracted at a nitrogen shift of 121.1 ppm. Data were zero-filled to 1024(t_1), 1024(t_2), and 4096(t_3) prior to Fourier transform, and processed with $\pi/2$-shifted sinebell apodization function in t_1, and with Lorentzian-to-Gaussian apodization function in the t_2 and t_3 dimensions (30 Hz of Lorentzian line narrowing and 60 Hz of Gaussian line broadening in t_2; 30 Hz of Lorentzian line narrowing and 70 Hz of Gaussian line broadening in t_3). First contour was cut at 4.4 times the noise rms, and each next was multiplied by a factor of 1.2. In this spectrum, both N[i+1]–CO[i]–CO[i+1] and N[i+1]–CO[i]–CO[i−1] correlations are clearly visible.

interactions, and attenuate polarization transfers. Finally, we could observe only two intraresidue carbonyl–carboxyl correlations in Asp22 and Asp40 in both the 2D $^{13}C'$–$^{13}C'$ (Fig. 5) and 3D NCOCO spectra. The internuclear carbonyl–carboxyl distances in other aspartates and glutamates, and backbone-side chain inter-carbonyl distances in glutamines and asparagines were either too long (more than 4 Å), or affected by local dynamics (e.g., D46, D47).

Table 1
Representative cross-peaks, their signal-to-noise ratios (SNR) and corresponding internuclear distances. Cross-peaks marked by asterisks are visible in the 2D spectrum in Fig. 7.

Cross-peak	C′–C′ distance (Å)	SNR
K10N-G9C′-K10C′	3.03	−29
K10N-G9C′-N8C′	3.27	−18
L12N-T1C′-K10C′	3.49	−16
*K13N-L12C′-T11C′	3.40	−19
*E15N-G14C′-E15C′	3.64	−14
*E15N-G14C′-K13C′	3.65	−8
K19N-T18C′-K19C′	3.35	−37
A20N-K19C′-T18C′	3.35	−32
*A23-D22C′-A23C′	3.08	−47
E24N-A23C′-D22C′	3.08	−21
A26N-T25C′-A26C′	3.00	−12
A26N-T25C′-E24C′	3.03	−26
*A29N-K28C′-E27C′	2.98	−17
*K31N-F30C′-A29C′	3.09	−20
*Q32N-K31C′-F30C′	2.99	−12
*Q32N-K31C′-Q32C′	3.01	−15
*Y33N-Q32C′-K31C′	3.01	−17
*Y33N-Q32C′-Y33C′	2.97	−16
*A34N-Y33C′-Q32C′	2.97	−17
*V39N-G38C′-V39C′	3.25	−43
W43N-V42C′-W43C′	3.52	−7
W43N-V42C′-G41C′	3.33	−24
E56N-T55C′-E56C′	3.25	−53

5. Conclusions and future developments

We have demonstrated in this work that efficient direct inter-carbonyl transfer can be achieved in proteins, and can be used to establish long-range interresidue correlations. Under experimental conditions used in this work, 22 kHz spinning rate and 600 MHz proton field strength, the HORROR recoupling condition shifts and anisotropically broadens to $\omega_{rf} > 1/2\omega_r$, with broadening inversely proportional to the spinning frequency. Matching this condition requires application of amplitude-modulated RF fields. The polarization transfer efficiency did not depend on the type of secondary structure and was on the order of 20–30% in both α-helical and β-sheet secondary motifs, where typical inter-carbonyl distances are 3 Å and 3.5 Å, respectively.

The 2D and 3D experiments presented in this work, although may be of use in peptides and small proteins with relatively uncongested spectra, will require further developments. In this respect, we have also attempted to extend the 3D NCOCO correlation experiment to include an additional polarization transfer from CO to aliphatic spins to establish long-range (e.g., N[i + 1]–CO[i]–(CO[i ± 1])–CA[i ± 1]) backbone correlations. Unfortunately, the sensitivity of such an experiment was not sufficient. The main reason, we believe, was the simultaneous presence of positive (e.g., N[i + 1]–CO[i]–CA[i]) and negative (e.g., N[i + 1]–CO[i]–CA[i + 1] and N[i + 1]–CO[i]–CA[i − 1]) correlations, which resulted in significant spectral overlap and cancelation of the cross-peaks. To remedy this situation, it should be possible to incorporate double-quantum filter (DQF) to eliminate the pseudo-diagonal peaks, to produce cross-peaks of the same sign, and to simplify spectra. The most attractive route towards this would be to use DREAM-based DQF [45]. As was estimated earlier, this would require 100 ms or longer mixing times to ensure adiabaticity of the transfer process. Although reaching such long mixing times appears to be problematic at the spinning rates of ∼20 kHz, the experiment would be much more feasible at faster spinning frequencies. With current probe technology spinning rates up to 70 kHz are achievable, and the CSA-induced broadening of Eq. (8) will reduce by a factor of ∼3, in turn reducing the required minimal mixing period length to about ∼30 ms. Given that low decoupling powers can be used at these spinning rates, we anticipate that much longer mixing could be applied without significant relaxation losses, allowing to approach the adiabatic limit.

Acknowledgments

We thank Dr. Ad Bax (NIH) for a generous gift of a plasmid encoding GB3, and Dr. C.P. Jaroniec and Mr. P. Nadaud (Ohio State University) for sharing the details of the GB3 purification protocol. This research was supported by the University of Guelph, the Natural Sciences and Engineering Research Council of Canada, the Canada Foundation for Innovation, and the Ontario Ministry of Research and Innovation. V.L. holds Canada Research Chair in Biophysics, and is a recipient of an Early Researcher Award from the Ontario Ministry of Research and Innovation. E.R. was supported by an undergraduate student research award. L.S. and A.G. are recipients of Ontario Graduate Scholarship.

References

[1] R.R. Ketchem, W. Hu, T.A. Cross, High-resolution conformation of gramicidin A in a lipid bilayer by solid-state NMR, Science 261 (1993) 1457–1460.
[2] S.J. Opella, F.M. Marassi, J.J. Gesell, A.P. Valente, Y. Kim, M. Oblatt-Montal, M. Montal, Structures of the M2 channel-lining segments from nicotinic acetylcholine and NMDA receptors by NMR spectroscopy, Nat. Struct. Biol. 6 (1999) 374–379.
[3] S.H. Park, A.A. Mrse, A.A. Nevzorov, M.F. Mesleh, M. Oblatt-Montal, M. Montal, S.J. Opella, Three-dimensional structure of the channel-forming trans-

membrane domain of virus protein "u" (Vpu) from HIV-1, J. Mol. Biol. 333 (2003) 409–424.
[4] M. Yi, T.A. Cross, H.X. Zhou, Conformational heterogeneity of the M2 proton channel and a structural model for channel activation, Proc. Natl. Acad. Sci. USA 106 (2009) 13311–13316.
[5] M. Baldus, Molecular interactions investigated by multi-dimensional solid-state NMR, Curr. Opin. Struct. Biol. 16 (2006) 618–623.
[6] M. Hong, Structure, topology, and dynamics of membrane peptides and proteins from solid-state NMR spectroscopy, J. Phys. Chem. B 111 (2007) 10340–10351.
[7] A. McDermott, Solid state NMR studies of enzymes and membrane proteins, Annu. Rev. Biophys. 38 (2009) 385–403.
[8] V.S. Bajaj, M.L. Mak-Jurkauskas, M. Belenky, J. Herzfeld, R.G. Griffin, Functional and shunt states of bacteriorhodopsin resolved by 250 GHz dynamic nuclear polarization-enhanced solid-state NMR, Proc. Natl. Acad. Sci. USA (2009).
[9] L. Shi, M.A.M. Ahmed, W. Zhang, G. Whited, L.S. Brown, V. Ladizhansky, Three-dimensional solid-state NMR study of a seven-helical integral membrane proton pump – structural insights, J. Mol. Biol. 386 (2009) 1078–1093.
[10] L. Shi, E.M. Lake, M.A. Ahmed, L.S. Brown, V. Ladizhansky, Solid-state NMR study of proteorhodopsin in the lipid environment: secondary structure and dynamics, Biochim. Biophys. Acta 1788 (2009) 2563–2574.
[11] A.B. Patel, E. Crocker, M. Eilers, A. Hirshfeld, M. Sheves, S.O. Smith, Coupling of retinal isomerization to the activation of rhodopsin, Proc. Natl. Acad. Sci. USA 101 (2004) 10048–10053.
[12] A. Lange, K. Giller, S. Hornig, M.F. Martin-Eauclaire, O. Pongs, S. Becker, M. Baldus, Toxin-induced conformational changes in a potassium channel revealed by solid-state NMR, Nature 440 (2006) 959–962.
[13] M. Hiller, L. Krabben, B.J. van Rossum, V. Kumar, W. Kuhlbrandt, H. Oschkinat, Solid-state MAS NMR of the outer-membrane protein g from *Escherichia coli*, FEBS J. 272 (2005) 373.
[14] M. Hiller, L. Krabben, K.R. Vinothkumar, F. Castellani, B.J. van Rossum, W. Kuhlbrandt, H. Oschkinat, Solid-state magic-angle spinning NMR of outer-membrane protein G from *Escherichia coli*, ChemBioChem 6 (2005) 1679–1684.
[15] Y. Li, D.A. Berthold, R.B. Gennis, C.M. Rienstra, Chemical shift assignment of the transmembrane helices of DsbB, a 20-kDa integral membrane enzyme, by 3D magic-angle spinning NMR spectroscopy, Protein Sci. 17 (2008) 199–204.
[16] M. Baldus, Spectral assignment of (membrane) proteins under magic angle spinning, in: A. Ramamoorthy (Ed.), NMR Spectroscopy of Biological Solids, Taylor & Francis Group, LLC, Boca Raton, FL, 2006, pp. 39–56.
[17] J. Pauli, M. Baldus, B. van Rossum, H. de Groot, H. Oschkinat, Backbone and side-chain C-13 and N-15 signal assignments of the alpha-spectrin SH3 domain by magic angle spinning solid-state NMR at 17.6 tesla, ChemBioChem 2 (2001) 272–281.
[18] W.T. Franks, K.D. Kloepper, B.J. Wylie, C.M. Rienstra, Four-dimensional heteronuclear correlation experiments for chemical shift assignment of solid proteins, J. Biomol. NMR 39 (2007) 107–131.
[19] M. Etzkorn, S. Martell, O.C. Andronesi, K. Seidel, M. Engelhard, M. Baldus, Secondary structure, dynamics, and topology of a seven-helix receptor in native membranes, studied by solid-state NMR spectroscopy, Angew. Chem. Int. Ed. 46 (2007) 459–462.
[20] M. Hong, K. Jakes, Selective and extensive C-13 labeling of a membrane protein for solid-state NMR investigations, J. Biomol. NMR 14 (1999) 71–74.
[21] V.A. Higman, J. Flinders, M. Hiller, S. Jehle, S. Markovic, S. Fiedler, B.J. van Rossum, H. Oschkinat, Assigning large proteins in the solid state: a MAS NMR resonance assignment strategy using selectively and extensively 13C-labelled proteins, J. Biomol. NMR 44 (2009) 245–260.
[22] B. Reif, M. Hohwy, C.P. Jaroniec, C.M. Rienstra, R.G. Griffin, NH-NH vector correlation in peptides by solid-state NMR, J. Magn. Reson. 145 (2000) 132–141.
[23] D. Marulanda, M.L. Tasayco, A. McDermott, M. Cataldi, V. Arriaran, T. Polenova, Magic angle spinning solid-state NMR spectroscopy for structural studies of protein interfaces. Resonance assignments of differentially enriched *Escherichia coli* thioredoxin reassembled by fragment complementation, J. Am. Chem. Soc. 126 (2004) 16608–16620.
[24] W.T. Franks, B.J. Wylie, S.A. Stellfox, C.M. Rienstra, Backbone conformational constraints in a microcrystalline U–N-15-labeled protein by 3D dipolar-shift solid-state NMR spectroscopy, J. Am. Chem. Soc. 128 (2006) 3154–3155.
[25] O.N. Antzutkin, J.J. Balbach, R.D. Leapman, N.W. Rizzo, J. Reed, R. Tycko, Multiple quantum solid-state NMR indicates a parallel, not antiparallel, organization of beta-sheets in Alzheimer's beta-amyloid fibrils, Proc. Natl. Acad. Sci. USA 97 (2000) 13045–13050.
[26] G.P. Drobny, J.R. Long, T. Karlsson, W. Shaw, J. Popham, N. Oyler, P. Bower, J. Stringer, D. Gregory, M. Mehta, P.S. Stayton, Structural studies of biomaterials using double-quantum solid-state NMR spectroscopy, Annu. Rev. Phys. Chem. 54 (2003) 531–571.
[27] M.A. Mehta, M.T. Eddy, S.A. McNeill, F.D. Mills, J.R. Long, Determination of peptide backbone torsion angles using double-quantum dipolar recoupling solid-state NMR spectroscopy, J. Am. Chem. Soc. 130 (2008) 2202–2212.
[28] Y. Ishii, C-13–C-13 dipolar recoupling under very fast magic angle spinning in solid-state nuclear magnetic resonance: applications to distance measurements, spectral assignments, and high-throughput secondary-structure determination, J. Chem. Phys. 114 (2001) 8473–8483.
[29] Z. Zheng, W. Qiang, D.P. Weliky, Investigation of finite-pulse radiofrequency-driven recoupling methods for measurement of intercarbonyl distances in polycrystalline and membrane-associated HIV fusion peptide samples, Magn. Reson. Chem. 45 (2007) S247–S260.
[30] N.C. Nielsen, H. Bildsoe, H.J. Jakobsen, M.H. Levitt, Double-quantum homonuclear rotary resonance – efficient dipolar recovery in magic-angle-spinning nuclear-magnetic-resonance, J. Chem. Phys. 101 (1994) 1805–1812.
[31] P.J. Carroll, P.L. Stewart, S.J. Opella, Structures of 2 model peptides – *N*-acetyl-D,L-valine and *N*-acetyl-L-valyl-L-leucine, Acta Crystallogr. C Crystal Struct. Commun. 46 (1990) 243–246.
[32] T.S. Ulmer, B.E. Ramirez, F. Delaglio, A. Bax, Evaluation of backbone proton positions and dynamics in a small protein by liquid crystal NMR spectroscopy, J. Am. Chem. Soc. 125 (2003) 9179–9191.
[33] W.T. Franks, D.H. Zhou, B.J. Wylie, B.G. Money, D.T. Graesser, H.L. Frericks, G. Sahota, C.M. Rienstra, Magic-angle spinning solid-state NMR spectroscopy of the beta 1 immunoglobulin binding domain of protein G (GB1): N-15 and C-13 chemical shift assignments and conformational analysis, J. Am. Chem. Soc. 127 (2005) 12291–12305.
[34] P.S. Nadaud, J.J. Helmus, C.P. Jaroniec, C-13 and N-15 chemical shift assignments and secondary structure of the B3 immunoglobulin-binding domain of streptococcal protein G by magic-angle spinning solid-state NMR spectroscopy, Biomol. NMR Assignments 1 (2007) 117–120.
[35] B.J. Wylie, L.J. Sperling, C.M. Rienstra, Isotropic chemical shifts in magic-angle spinning NMR spectra of proteins, Phys. Chem. Chem. Phys. 10 (2008) 405–413.
[36] A. Pines, M.G. Gibby, J.S. Waugh, Proton-enhanced NMR of dilute spins in solids, J. Chem. Phys. 59 (1973) 569–590.
[37] A.E. Bennett, C.M. Rienstra, M. Auger, K.V. Lakshmi, R.G. Griffin, Heteronuclear decoupling in rotating solids, J. Chem. Phys. 103 (1995) 6951–6958.
[38] B.M. Fung, A.K. Khitrin, K. Ermolaev, An improved broadband decoupling sequence for liquid crystals and solids, J. Magn. Reson. 142 (2000) 97–101.
[39] S.R. Hartmann, E.L. Hahn, Nuclear double resonance in the rotating frame, Phys. Rev. 128 (1962) 2042–2053.
[40] M. Baldus, A.T. Petkova, J. Herzfeld, R.G. Griffin, Cross polarization in the tilted frame: assignment and spectral simplification in heteronuclear spin systems, Mol. Phys. 95 (1998) 1197–1207.
[41] L. Shi, X. Peng, M.A. Ahmed, D.A. Edwards, L.S. Brown, V. Ladizhansky, Resolution enhancement by homonuclear *J*-decoupling: application to three-dimensional solid-state magic angle spinning NMR spectroscopy, J. Biomol. NMR 41 (2008) 9–15.
[42] F. Delaglio, S. Grzesiek, G.W. Vuister, G. Zhu, J. Pfeifer, A. Bax, NMRpipe – a multidimensional spectral processing system based on unix pipes, J. Biomol. NMR 6 (1995) 277–293.
[43] R. Keller, The Computer Aided Resonance Assignment Tutorial, CANTINA Verlag, Goldau, 2004.
[44] C.R. Morcombe, K.W. Zilm, Chemical shift referencing in MAS solid state NMR, J. Magn. Reson. 162 (2003) 479–486.
[45] R. Verel, M. Baldus, M. Ernst, B.H. Meier, A homonuclear spin-pair filter for solid-state NMR based on adiabatic-passage techniques, Chem. Phys. Lett. 287 (1998) 421–428.
[46] R. Verel, M. Ernst, B.H. Meier, Adiabatic dipolar recoupling in solid-state NMR: the DREAM scheme, J. Magn. Reson. 150 (2001) 81–99.
[47] U. Haeberlen, J.S. Waugh, Coherent averaging effects in magnetic resonance, Phys. Rev. 175 (1968) 453–467.
[48] S. Dusold, A. Sebald, Dipolar recoupling under magic-angle spinning conditions, Annu. Rep. NMR Spectrosc. 41 (2000) 185–264.
[49] A. Wokaun, R.R. Ernst, Selective excitation and detection in multilevel spin systems: application of single transition operators, J. Chem. Phys. 67 (1977) 1752–1758.
[50] S. Vega, Fictitious spin 1/2 operator formalism for multiple quantum NMR, J. Chem. Phys. 68 (1978) 5518–5527.
[51] Z.H. Gan, D.M. Grant, R.R. Ernst, NMR chemical shift anisotropy measurements by RF driven rotary resonance, Chem. Phys. Lett. 254 (1996) 349–357.
[52] J.P. Derrick, D.B. Wigley, The third IgG-binding domain from streptococcal protein G. An analysis by X-ray crystallography of the structure alone and in a complex with Fab, J. Mol. Biol. 243 (1994) 906–918.